Original Article

Cdc42 is essential for both articular cartilage degeneration and subchondral bone deterioration in experimental osteoarthritis[†]

Running title: Cdc42 in osteoarthritis

Xinhua Hu,[1,*] Xing Ji,[1,*] Mengting Yang,[1] Shihao Fan,[1] Jirong Wang,[1] Meiping Lu,[2] Wei Shi,[1] Liu Mei,[1] Chengyun Xu,[1] Xueying Fan,[1] Musaddique Hussain,[1] Jingyu Du,[3] Junsong Wu,[3,†] Ximei Wu[1,†]

[1]Department of Pharmacology, Zhejiang University School of Medicine, Hangzhou 310058, China

[2]Department of Rheumatology of the Children's Hospital, Zhejiang University School of Medicine, Hangzhou 310003, China

[3]Department of Orthopedics of the First Affiliated Hospital, Zhejiang University School of Medicine, Hangzhou 310003, China.

*These authors contribute equally to the work.

[†]Corresponding author:

Ximei Wu Prof., M.D., Ph.D.
Department of Pharmacology, Zhejiang University School of Medicine, 866 Yuhangtang Road, Hangzhou, 310058, China. Tel/Fax: +86-571-8898-1121. E-mail: xiwu@zju.edu.cn

Junsong Wu Prof., M.D., Ph.D.
Department of Orthopedics of the First Affiliated Hospital, Zhejiang University School of Medicine, Hangzhou 310003, China. 79 Qingchun Road, Hangzhou, 310003, China. Tel/Fax: +86-571-8723-6125. E-mail: wjs128@sina.com

[†]This article has been accepted for publication and undergone full peer review but has not been through the copyediting, typesetting, pagination and proofreading process, which may lead to differences between this version and the Version of Record. Please cite this article as doi: [10.1002/jbmr.3380]

Additional Supporting Information may be found in the online version of this article.

Initial Date Submitted August 17, 2017; Date Revision Submitted December 15, 2017; Date Final Disposition Set December 29, 2017

Journal of Bone and Mineral Research

DOI 10.1002/jbmr.3380

ABSTRACT

Cdc42, a member of Rho family small GTPases, is critical for cartilage development. We investigated the roles of Cdc42 in osteoarthritis and explored the potential mechanism underlying Cdc42-mediated articular cartilage degeneration and subchondral bone deterioration. Cdc42 is highly expressed in both articular cartilage and subchondral bone in a mouse osteoarthritis model with surgical destabilisation of the medial meniscus (DMM) in the knee joints. Specifically, genetic disruption of *Cdc42*, knockdown of Cdc42 expression, or inhibition of Cdc42 activity robustly attenuates the DMM-induced destruction, hypertrophy, high expression of matrix metallopeptidase-13 and collagen X, and activation of Stat3 in articular cartilages. Notably, genetic disruption of *Cdc42*, knockdown of Cdc42 expression or inhibition of Cdc42 activity significantly restored the increased numbers of mesenchymal stem cells, osteoprogenitors, osteoblasts, osteoclasts, and neovascularised vessels, the increased bone mass, and the activated Erk1/2, Smad1/5 and Smad2 in subchondral bone of DMM-operated mice. Mechanistically, Cdc42 mediates interleukin-1β-induced interleukin-6 production and subsequent Jak/Stat3 activation to regulate chondrocytic inflammation, and also lies upstream of Erk/Smads to regulate subchondral bone remodelling during transform growth factor-β1 signalling. Cdc42 is apparently required for both articular cartilage degeneration and subchondral bone deterioration of osteoarthritis, thus, interventions targeting Cdc42 have potential in osteoarthritic therapy.

KeyWords: Osteoarthritis; Cdc42; Articular cartilage; Subchondral bone

This article is protected by copyright. All rights reserved

Introduction

Osteoarthritis (OA) is a leading cause of chronic disability and a most common joint disease characterised by the degeneration of articular cartilage, subchondral bone sclerosis, osteophyte formation, osteochondral angiogenesis and joint inflammation.[1,2] Previous studies on OA primarily focused on articular cartilage degeneration; however, the discrepancy in results between preclinical studies and clinical treatments for OA suggests that targeting articular cartilage alone is not sufficient to halt the progression of OA.[1,2] Accumulating evidence now indicates that articular cartilage and subchondral bone form a holistic unit and mutually manage peripheral biochemical and biomechanical stress. OA is therefore considered a disease of the whole joint and is classically accompanied by subchondral bone remodelling.[3-6]

Patients with OA exhibit high levels of interleukin-1β (IL-1β) in the articular cartilage and other elements of the joint.[7,8] IL-1β is one of the two major cytokines involved in OA onset and development, and it also plays a critical role in the pathogenesis of other types of arthritis.[7] IL-1β induces the production of pro-inflammatory cytokine, such as IL-6, promotes catabolism, and inhibits anabolism in articular cartilage. Therefore, inhibiting IL-1β signalling, especially to decrease matrix metalloproteinase (MMP) activities, is crucial for the development of OA therapy.[8,9] Accumulating evidence suggests that aberrantly high signalling activity of transforming growth factor-β (TGF-β) in subchondral bone induces abnormal recruitment of nestin+ mesenchymal stem cells (MSCs), resulting in the formation of osteoid islets, an accompanying angiogenesis and final sclerosis of subchondral bone in OA.[5] Inhibition of this signalling pathway in subchondral bone may therefore provide a potential avenue for OA therapy.

The members of the Rho family of small GTPases, including Rac1, Cdc42, and RhoA, are molecular switches that cycle between inactive GDP-bound and active GTP-bound forms and regulate the cytoskeleton and multiple cell functions, including cartilage biology.[10-15] Our most recent and other previous studies indicate that Cdc42 is critical for chondrogenesis, including the mesenchymal condensation, lifespan of the chondrocytes and chondrogenic differentiation during long bone development.[11-13] Conditional deletion of *Cdc42* in limb mesenchymal progenitors causes a delayed mesenchymal condensation and generation of a variety of bone phenotypes.[11,12] Severe defects in long bone growth plate cartilage is related to loss of columnar organisation of chondrocytes, as well as thickening and massive accumulation of hypertrophic chondrocytes, resulting in delayed endochondral bone formation associated with reduced bone growth.[11,12] Chondrocyte-specific disruption of *Cdc42* also causes severe defects in growth plate chondrocytes of long bones, characterised by a reduced proliferating zone height, wider hypertrophic zone, and loss of columnar organisation in proliferating chondrocytes.[13]

Despite the importance of Cdc42 in cartilage development, *Cdc42* loss of function results in osteopetrosis and resistance to ovariectomy-induced bone loss in mice, as Cdc42 regulates bone modelling and remodelling by modulating receptor activator of nuclear factor κB ligand (RANKL)/macrophage colony-stimulating factor (M-CSF) signalling and osteoclast polarisation.[16] Cdc42 mediates a Rho-family GTPase activation cascade for the formation of the endothelial cell filopodial protrusions necessary for tubule remodelling, thereby influencing endothelial construction and angiogenesis.[17] Furthermore, Cdc42 participates in inflammatory signalling pathways to regulate chondrocytic phenotypes.[11,18]

The fundamental roles of Cdc42 in chondrogenesis, osteoclastogenesis, osteoblastogenesis, and angiogenesis lead us to speculate that Cdc42 could be implicated in the development of OA. In the present study, we demonstrate that Cdc42 is required for both articular cartilage degradation and subchondral bone deterioration in a mouse OA model with surgical destabilisation of the medial meniscus (DMM) in the knee joints, and also provide new insights into the mechanisms of Cdc42 action that may have therapeutic implications for OA.

Materials and Methods

Mouse strains and treatments

Three-month-old male C57BL/6J mice were purchased from Shanghai SLAC Laboratory Animal Co. (License No. SCXK 2003-0003, Shanghai, China). *Cdc42*$^{flox/flox}$ mice on a C57BL/6J genetic background were provided by Dr. Yi Zheng from Cincinnati Children's Hospital Medical Center.[19] All mice were maintained at specific pathogen free animal care facility of Zhejiang University and housed in a room at 23 ± 2°C, with 50 ± 10% humidity and a 12-h light:12-h dark cycle (lights on from 8:00 a.m. to 8:00 p.m.). All mice were allowed free access to water and regular rodent chow. All protocols of mouse procedures were approved by the Ethics Committee of Zhejiang University. The DMM surgery at knee joint model of OA and sham surgery were performed in the wild-type and *Cdc42*$^{flox/flox}$ mice anaesthetize with 20% urethane (Sigma, St. Louis, MO) as previously described.[20] ZCL278 (Selleck, Huston, TX), a selective Cdc42 inhibitor, was intra-articularly injected at 8 μg per knee joint three times a week, starting from 10 days post DMM surgery, and the control knee joint was injected with the same volume of 0.1% dimethyl sulfoxide (DMSO) in PBS. Scramble- or Cdc42-shRNA-expressing lentiviruses (Biotool, Shanghai, China) with the titer of 1×10^7 clone formation units per ml were intra-articularly administered into C57BL/6J mice at 5 μl per joint, once a week starting from 10 days post DMM surgery. Green fluorescent protein (GFP)- or GFP-Cre-adenoviruses (Biotool) with titer of 1×10^8 plaque forming units per ml were intra-articularly injected into *Cdc42*$^{flox/flox}$ mice at 5 μl per joint once a week starting from 10 days post DMM surgery. The microinjection was performed with 5 μl microinjector (Hamilton Company, Reno, NV) and 33 gauge needles(Hamilton

Company). Mice were euthanized at 4, 8 and 12 weeks post DMM and used to assess the severity of OA.

Isolation of primary articular chondrocytes

Primary articular chondrocytes (PACs) were prepared from sixty C57BL/6J mice at 5-d-old as previously described.[21] Briefly, skin and soft tissues were removed from the hind legs of euthanized mice and the soft tissue of the joints was discarded to isolate the femoral heads, condyles and tibial plateaux. Then, the cartilage pieces were washed and incubated with 3 mg/ml of collagenase D (Sigma) in Dulbecco's Modified Eagle's medium (DMEM, Sigma) containing 2 mM L-glutamine, 50 U/ml penicillin G and 0.05 mg/ml streptomycin for 45 min at 37 °C in a thermal incubator under 5% CO_2. After retrieved and agitated, the cartilage pieces were further digested in 0.5 mg/ml collagenase D solution over night. The cell aggregates were pipetted and dispersed to yield a suspension of isolated cells, and the cell suspension was then filtered through a sterile 48 μM cell strainer. After centrifugation at 400g for 10 min, the pellet was washed and resuspended into DMEM medium containing 10% fetal bovine serum (FBS, Life Technologies, Grand Island, NY). The PACs were counted and subjected to a quick trypan blue exclusion test. 1×10^6 (on average) PACs were obtained per mouse, of which >97% exclude trypan blue. PACs were seeded on a culture dish at density of 1×10^4 cells/cm^2 for the following experiments.

Cell cultures and treatments

C3H10T1/2 and ATDC5 cells were obtained from American Type Culture Collection (Manassas, VA) and cultured as previously described.[11] PACs, ATDC5 cells or C3H10T1/2 cells were treated with recombinant mouse IL-1β (PeproTech, Rocky Hill, NJ) at 10 ng/ml, recombinant mouse IL-6 (PeproTech) at 10 ng/ml or recombinant

human TGF-β1 (PeproTech) at 5 ng/ml for 30 or 60 min, and IL-6 neutralizing antibody (IL-6ab, Novus Biologicals, Littleton, CO) at 5 ng/ml was incubated 2 h before and during IL-1β treatments. PACs were starved overnight and then treated with recombinant mouse IL-1β at 10 ng/ml for the indicated times, ZCL278 and IPA-3 (sigma) were treated 2 h before and during IL-1β treatments. C3H10T1/2 cells were starved for 16 h and then treated with recombinant human TGF-β1 at 5 ng/ml for the indicated times, and inhibitors including ZCL278 and PD98059 (Sigma) were treated 2 h before and during TGF-β1 treatments. Alternatively, C3H10T1/2 cells were transfected with Cdc42 or caCdc42 plasmid and then treated with or without indicated concentration of PD98059 for 1 h.

Hypertrophy, osteoblastogenic and chondrogenic differentiation assays

Hypertrophy assay were performed in the ATDC5 cells and PACs. ATDC5 cells and PACs were treated with and without ZCL278 for 21 and 14 days, respectively, in the absence or presence of hypertrophic medium (HM) containing 1nM dexamethasone, 20mM β-glycerophosphate, 50 μg/ml ascorbate,50 ng/ml thyroxin and 1%ITS, and then stained with 1% Alizarin Red S (Sigma) solution with pH 4.2.[11,22] Alkaline phosphatase (ALP) staining and activity determination were performed in C3H10T1/2 cells as described previously.[22] Cells were treated with and without ZCL278 for 7 days or transfected with or without constitutively active form of Cdc42 (caCdc42, G12V) for 72 h in the absence or presence of osteoblast differentiation medium (OBM) containing 50 mM ascorbic acid, 100 nM dexamethasone and 10 mM β-glycerophosphate. Bone marrow stromal cells (BMSCs) isolation and mineralization assay were performed as described previously.[22] Chondrogenic differentiation was evaluated in ATDC5 cells. ATDC5 cells were maintained with

complete growth medium containing 1% insulin-transferrin-selenium (ITS) liquid media supplement (Sigma) and 50 ng/ml ascorbic acid for 14 days, and then stained with 0.1% Alcian Blue (Sigma).

Western blotting assays

Western blot was performed as previously described.[11] Protein extracts were prepared in whole cell lysis buffer with an inhibitor mixture (Sigma). Protein concentrations were determined using a Bradford Protein Assay Kit (Beyotime, Shanghai, China), and 30 μg of total protein was subjected to SDS-PAGE followed by a transfer onto PVDF membranes (Millipore, Bedford, MA). Membranes were incubated with phosphorylated antibodies, before stripped and further re-probed with non-phosphorylated antibodies. Primary antibodies include p-Smad2, p-Smad1/5, Smad5 (CST, Danvers, MA), signal transducer and activator of transcription 3 (Stat3), p-Stat3, extracellular signal-regulated kinases 1 and 2 (Erk), p-Erk, c-Jun N-terminal kinase (JNK), p-JNK, P38 mitogen-activated protein kinases (P38), p-P38 , Janus-activated kinase 1 (Jak1), Jak2, p-Jak1, p-Jak2 (all from CST), glyceraldehyde 3-phosphate dehydrogenase (GAPDH), Myc (all from Santa Cruz Biotechnology, Santa Cruz, CA), GFP, MMP13, collagen X (COLX) and Cdc42 (from Abcam, Cambridge, UK). The IRDye 680 and 800 second antibodies were from LI-COR Bioscience (Lincoln, Nebraska). The signals were visualized with Odyssey Infrared Imaging System (LI-COR, Lincoln, NE). GAPDH was used as internal standard of total target proteins, and phosphorylated proteins were normalised to their total proteins, respectively. Immunoreactive bands from triplicates (n=3) were quantified by image software (ImageJ, http://rsb.info.nih.gov/ij/download.html) obtained from National Institutes of Health and the mean intensity from first band was set to 1.

Cdc42 activation assay

Cells were harvested for preparation of cell lysates and centrifugation. The supernatants were then subjected to Cdc42 pull-down assays by using Active GTPase Pull-Down and Detection kits (Pierce Biotechnology, Rockford, IL) as previously described.[23] The GTP bound form of Cdc42 (GTP-Cdc42) was active form of Cdc42, and the total Cdc42 was used as an internal control for active form of Cdc42.

Immunoprecipitation

For co-immunoprecipitation, cells were transfected with Cdc42 or caCdc42 expressing vectors and starved for 12h. Immunoprecipitation were performed using standard protocols. After treatments, cells were harvested for preparation of cell lysates and centrifugation, the supernatant was subjected to immunoprecipitation by using protein A/G plus agarose beads (Santa Cruz Biotechnology) containing either control IgG or anti-Myc antibody. After beads were washed with washing buffer (10mM Tris-HCl, pH 8.0, 150mM NaCl, 10% glycerol, 1% NP-40, and 2mM EDTA), the sample was boiled and centrifuged, the supernatant was subjected to SDS-PAGE and western blotting.

Quantification of mRNA by real-time polymerase chain reaction

Total RNA was isolated from cells using TRIzol reagent (Takara, Dalian, China). Messenger RNA levels of ALP, bone morphogenetic protein 2 (BMP2), BMP4, collagen1α1 (Col1a1), collagen2α1(Col2a1), COLX, cyclooxygenase-2 (Cox2), inducible nitric oxide synthase (iNOS), IL-6, MMP13, Osterix (OSX), and Runt-related transcription factor 2 (Runx2) were determined by quantitative real-time polymerase chain reaction (qRT-PCR) as described previously.[11] The relative amounts of each mRNA level were normalised to control GPADH and β-actin levels,

the differences in mRNA levels were calculated by $2^{-\Delta\Delta Ct}$ method. The primers used in qRT-PCR were presented in the Supporting Table 1.

ELISA assay

PACs were incubated with IL-1β at 10 ng/ml for the indicated times or 1h, inhibitors including ZCL278 at 50 μM and IPA-3 at 20 μM were treated 2 h before and during IL-1β treatments. The culture media were harvested for determination of IL-6 by a Mouse IL-6 Quantikine ELISA Kit (R&D systems, Minneapolis, MN) with sensitivity1.8 pg/ml, assay range 7.8-500 pg/ml, and cross-reactivity < 0.5%. The protein levels in the culture media were determined by Bradford Protein Assay Kit. The amounts of IL-6 were normalised to the 100 μg protein in culture media of PACs.

Immunostaining and histomorphometry analyses

Knee joints were harvested and fixed in 10% neutral formalin for 72 h at 4 °C. After μCT scanning, intact knee joints were decalcified in 14% EDTA for 21 days on a shaker at 4 °C and embedded in paraffin for sectioning at 4 μm. For H&E, safranin-O and fast green staining, coronal sections were performed through the entire joint at approximately 80 μm intervals, and it is usual to obtain 13-15 slides per knee joint. Cartilage destruction was scored using a modified osteoarthritis research society international (OARSI) scoring system as previously described.[24] The scores of the top eight consecutive sections were added together to give the summed score. Under two-blind method, the OA severity was defined as summed and/or maximal scores for each knee joint. The sagittal sections (4 μm) for the subchondral bone area were derived from the middle of tibias. Sections were used for tartrate-resistant acid phosphatase (Trap) staining and immunostaining with a standard protocol. Primary antibodies included nestin, osterix, p-Smad1/5, MMP13, COLX, ALP, vascular

endothelial growth factor receptor 2 (VEGFR2), and GFP (all from Abcam), Col2a1, p-Smad2 (NovusBio), p-Stat3, p-Erk (all from CST). Horse radish peroxidase (HRP)-labeled secondary antibody was used to detect immunohistochemical staining followed by counterstaining with hematoxylin. Alexa-Fluor 488 or 546 flourescence dyes (Life Technologies, Grand Island, NY) were used for immunofluorescent staining followed by counterstaining with DAPI. Tartrate-resistant acid phosphatase (Trap) staining was performed by using Leukocyte Trap Kit (Sigma) as described previously.[22] We counted the number of positively stained cells in the whole tibia subchondral bone area or articular cartilage per specimen in five sequential sections per mouse in each group. Quantification was performed in a blinded manner using OsteoMeasureXP Software (OsteoMetrics, Inc., Decatur, GA) and IPP 6.0 (Media Cybernetics, Inc., Rockville, MD).

μCT measurements

We dissected knee joints from mice free of soft tissue, preserved them in 70% ethanol and analyzed them by high-resolution μCT (Skyscan1176).[23,25] We reconstructed and analyzed images using NRecon v1.6 and CTAn v1.15, respectively. XYZ axes were adjusted by Dataviewer V1.5. Three-dimensional model visualization software, CTVol v2.2, was used to analyze parameters of the trabecular bone in the epiphysis. The scanner was set at a voltage of 50 kV with a current of 500 μA and a resolution of 9 μm per pixel. Sagittal images of the tibiae subchondral bone were used to perform three-dimensional histomorphometric analyses. We defined the region of interest to cover the whole subchondral bone medial compartment and used a total of 40 consecutive images from the medial tibial plateau for three-dimensional reconstruction and analysis. Three-dimensional structural parameters including trabecular separation (Tb.Sp), subchondral bone plate thickness (SBP.Th), bone

volume/trabecular volume (BV/TV), and trabecular number (Tb.N) were analyzed as previously described.[25]

Statistical analysis

Numerical data were presented as mean ± SEM. For multi-factorial comparisons, One-way ANOVA and Tukey–Kramer multiple comparisons test was used. $p<0.05$ was considered statistical significance. All data analysis was conducted with SPSS statistical package (IBM, North Castle, NY).

Results

Cdc42 is highly expressed in articular cartilage and subchondral bone and participates in chondrocytic differentiation and hypertrophy

We determined the expression patterns of Cdc42 in mice with experimental OA by immunostaining the sections of knee joints after DMM or sham surgery. Cdc42 was moderately expressed in the calcified cartilage, but not in the articular cartilage, of knee joints in normal mice and in mice that underwent sham surgery; however, DMM surgery caused a substantial increase in Cdc42 expression in both articular and calcified cartilage (Fig. 1*A*). Likewise, Cdc42 was expressed frequently at the surface of subchondral bone but rarely in the subchondral bone marrow of the tibias of normal or sham-operated mice, whereas mice that underwent DMM surgery showed a robust enhancement of Cdc42 expression in the bone marrow but not at the surface of subchondral bone (Fig. 1*A*). The expression patterns of Cdc42 in knee joints of mice with experimental OA therefore suggested a potential importance for Cdc42 in both articular degradation and subchondral bone remodelling.

We examined the potential roles of Cdc42 in chondrocytic differentiation and hypertrophy by culturing ATDC5 pre-chondrocytes and PACs in the presence or absence of ZCL278, a specific Cdc42 inhibitor. PACs had typical articular chondrocyte phenotypes, including obvious chondrocytic morphology with Col2a1 expression, passage-dependent alterations in both Col2a1 and Col1a1 mRNA levels, and characterized Alcian blue staining (Supporting Fig. 1*A*-*D*). ZCL278 had no effect on the Alcian Blue staining of ATDC5 cells in response to ITS medium or on the Alizarin Red S staining of PACs and ATDC5 cells in response to hypertrophy medium (HM); however, ZCL278 significantly enhanced ITS-induced Alcian Blue staining in ATDC5 cells and robustly diminished HM-induced Alizarin Red S

staining in both PACs and ATDC5 cells (Supporting Fig. 2*A* and Fig. 1*B*). Thus, inhibition of Cdc42 activity promoted chondrocytic differentiation and suppressed chondrocytic hypertrophy.

Cdc42 mediates IL-1β-induced chondrocytic inflammation

We investigated the potential roles of Cdc42 in IL-1β-triggered chondrocytic inflammation. IL-1β at 10 ng/ml caused significant increases in the GTP-bound form of Cdc42 (GTP-Cdc42, active form) but did not affect the total Cdc42 in PACs (Fig. 1*C*). IL-1β caused a time-dependent induction of protein levels of p-Jak1, p-Jak2, and p-Stat3, whereas ZCL278 at 50 μM almost completely abolished the IL-1β-induced these protein levels in PACs (Fig. 1*D*). Likewise, inhibition of p21-activated kinase (Pak), a downstream effector of Cdc42,[11] by IPA-3 at 10 and 20 μM almost completely abolished IL-1β-induced p-Jak1/2 as well as p-Stat3 levels in PACs (Fig. 1*E*). Moreover, IL-1β caused a significant induction of the mRNA (in PACs and ATDC5 cells) and protein (in ATDC5 cells) expression of both MMP13 and COLX, the respective markers for articular cartilage degradation and chondrocytic hypertrophy, whereas ZCL278 dose-dependently reduced the basal as well as IL-1β-induced these mRNA and protein expression (Fig. 1*F, G*; Supporting Fig. 2*B-D*). Finally, ZCL278 dose-dependently suppressed the IL-1β-induced mRNA expression of iNOS and Cox2, the catabolic markers of articular chondrocytes in PACs (Supporting Fig. 2*E, F*). We next examined the synergistic effects of Cdc42 and Pak in IL-1β-induced chondrocytic degradation and hypertrophy. Though ZCL278 at 20 μM or IPA-3 at 2.5 μM slightly suppressed both the Stat3 activation and mRNA expression of MMP13 and COLX in response to IL-1β stimulation, the combination of ZCL278 and IPA-3 produced a significantly synergistic effect on the suppression

of Stat3 activation as well as these mRNA expression (Fig. 1*H-J*). Moreover, overexpression of caCdc42 robustly induced COLX and MMP13 protein expression in ATDC5 cells, whereas inhibition of Pak activity by IPA-3 almost completely abolished caCdc42-induced these protein expression (Supporting Fig. 2*G*). Thus, Cdc42 in conjunction with Pak induced a signalling module composed of Jak/Stat3 in articular chondrocytic inflammation in response to IL-1β.

Cdc42 mediates IL-1β-induced IL-6 production and Jak/Stat3 activation

IL-1β began to activate Jak/Stat3 at 1 hour after treatment, and IL-6, a target of IL-1β signalling, but not IL-1β was believed to activate Jak/Stat3 signalling.[7-9] We next determined whether Cdc42 mediated the IL-6 production and subsequent Jak/Sta3 activation. In PACs, IL-1β at 10 ng/ml significantly induced both the mRNA and protein expression of IL-6, while inhibition of either Cdc42 by ZCL278 or Pak by IPA-3 robustly attenuated IL-6 production in response to IL-1β stimulation (Fig. 2*A-D*). Although IL-6 did not affect the Cdc42 activation and IL-6ab did not affect the IL-1β-induced Cdc42 activation either, IL-6ab did completely abolish IL-1β-induced Jak/Stat3 activation (Fig. 2*E-G*). Thus, IL-1β activated Cdc42/Pak to induce the production of IL-6 that subsequently activated Jak/stat3 in articular chondrocytes.

Cdc42 mediates TGF-β1-induced osteoblastogenesis

We investigated the potential roles of Cdc42 in osteoblastogenesis in response to TGF-β1 by culturing C3H10T1/2 cells, a cell line of murine embryonic fibroblast. TGF-β1 at 5 ng/ml caused a significant increase in GTP-Cdc42, but did not affect the total Cdc42 levels (Fig. 3*A*). TGF-β1 increased p-p38 and p-Erk but not p-JNK levels, whereas ZCL278 at 20 and 50 μM completely abolished TGF-β1-induced increases in

these protein levels (Fig. 3*B*, *C*; Supporting Fig. 2*H*). Likewise, TGF-β1 robustly increased p-Smad1/5 and p-Smad2/3 levels, but ZCL278, at 10 to 50 μM, dose-dependently diminished the TGF-β-induced these protein levels (Fig. 3*D*). PD98059, an Erk inhibitor, at 10 to 40 μM, dose-dependently reduced the TGF-β1-induced p-Smad1/5 and p-Smad2/3 levels (Fig. 3*E*). Overexpression of Cdc42 and caCdc42 enhanced p-Erk expression, but not p-P38 expression, whereas PD98059 completely abolished the caCdc42-induced p-Smad1/5 levels and largely attenuated the caCdc42-induced p-Smad2/3 levels (Fig. 3*F*, *G*). Moreover, the protein complex immunoprecipitated by a Myc antibody in C3H10T1/2 cells overexpressing Myc-tagged Cdc42 or caCdc42 contained p-Erk2, though overexpression of caCdc42 resulted in a greater p-Erk2 content in the immunocomplex than did overexpression of Cdc42 (Fig. 3*H*). Furthermore, ZCL278 at 50 μM significantly diminished TGF-β1-induced mRNA levels of osteoblastogenic markers, including ALP and osterix, as well as OBM-induced ALP staining and activity (numerical data); conversely, overexpression of caCdc42 in C3H10T1/2 cells robustly enhanced ALP staining and activity (Fig. 3*I-K*). Finally, though ZCL278 did not affect the basal BMP2 and BMP4 and TGF-β1-negated BMP4 mRNA expression in C3H10T1/2 cells, ZCL278 consistently attenuated not only the mRNA expression of osteoblastogenic markers, including Runx2 and Col1a1, in response to TGF-β1 but also the mineralization in response to OBM in primary BMSCs (Fig. 3*L*, *M*; Supporting Fig. 3). Taken together, these results showed that Cdc42 participated in the formation of a signalling module composed of TGF-β1-Cdc42-Erk-Smads and subsequently mediated TGF-β1-induced osteoblastogenesis.

Genetic disruption of *Cdc42* attenuates articular cartilage degradation in mice with experimental OA

We investigated the potential roles of Cdc42 in mice with experimental OA by intra-articular instillation of adenoviruses expressing GFP or GFP-Cre recombinase into *Cdc42*$^{flox/flox}$ mice after sham (sham/GFP or sham/Cre mice) or DMM (DMM/GFP or DMM/Cre mice) operations. GFP was diffusely expressed at relatively low levels in the medial tibial plateau and femoral condyle, but robustly expressed in the subchondral bone in both sham- and DMM-operated mice, resulting in a significant attenuation of Cdc42 expression in both sham/Cre and DMM/Cre mice (Fig. 4*A, E, K*). Thus, intra-articular administration of GFP-Cre-expressing adenoviruses effectively disrupted the *Cdc42* expression in articular cartilage of *Cdc42*$^{flox/flox}$ mice.

The cartilage integrity at 12 weeks post-DMM was histologically assessed and scored according to the modified OARSI scoring system. The articular cartilage of DMM/GFP mice showed an apparent loss of cartilage integrity, including loss of Safranin O-fast green staining, accompanied by increases in hypertrophic cell numbers and thinning of the cartilage, when compared with sham/GFP mice (Fig. 4*B-D*). Consistent with the histological alterations, the modified OARSI scoring indicated significantly lower hyaline cartilage (HC) thickness and higher calcified cartilage (CC) thickness, summed scores (SS), and maximal scores (MS) in DMM/GFP mice than in sham/GFP mice (Fig. 4*I, J*). As expected, GFP-Cre-adenovirus instillation restored the loss of cartilage integrity in DMM-operated mice when compared with GFP-adenovirus instillation (Fig. 4*B-D*). In agreement with the histological alterations, the modified OARSI scoring indicated that GFP-Cre-adenovirus instillation apparently normalised histological scores in

DMM-operated mice at 12 weeks post-surgery when compared with GFP-adenovirus (Fig. 4*B-D, I, J*). The effects of GFP- and GFP-Cre-adenoviruses on MMP13, COLX, and p-Stat3 (an effector of IL-6 signalling) expression in mice at 12 weeks post-operation were examined by immunostaining. DMM/GFP mice exhibited significantly increased levels of MMP13, COLX and p-Stat3 in articular and calcified cartilages when compared with sham/GFP mice, but DMM/Cre mice showed significantly attenuated MMP13, COLX and p-Stat3 levels when compared with DMM/GFP mice (Fig. 4*F-H, K*). Thus, in agreement with the *in vitro* observations, genetic disruption of *Cdc42* in articular cartilage attenuated IL-1β-induced IL-6 signalling as well as chondrocytic inflammation and hypertrophy.

Genetic disruption of *Cdc42* attenuates subchondral bone deterioration in mice with experimental OA

We dissected the roles of Cdc42 in subchondral bone remodelling of *Cdc42*$^{flox/flox}$ mice with experimental OA by immunostaining, μCT examination and semi-quantification. Immunostaining for Cdc42 indicated a significantly lower Cdc42 expression in sham/Cre and DMM/Cre mice than in their respective controls (Fig. 5*A, K*). Immunostaining for nestin, which is primarily expressed in adult bone marrow MSCs,[5] revealed that DMM/Cre mice had significantly decreased numbers of nestin$^+$ cells when compared with DMM/GFP mice (Fig. 5*B, L*). Once committed to the osteoblast lineage, MSCs express osterix, a marker of osteoprogenitors.[5] The number of osterix$^+$ osteoprogenitors and ALP$^+$ osteoblasts in the subchondral bone marrow were significantly decreased in DMM/Cre mice when compared with DMM/GFP mice (Fig. 5*C, D, K, L*). These results indicated that nestin$^+$ MSCs undergo osteoblastic differentiation for de novo bone formation.

We also measured angiogenesis by immunostaining for VEGFR2. DMM/Cre mice showed significant decreases in VEGFR2$^+$ cell numbers when compared with DMM/GFP mice (Fig. 5*E, L*). We further investigated the *in vivo* roles of Cdc42 in TGF-β1 signalling in subchondral bone areas. Immunostaining indicated that p-Erk1/2$^+$, p-Smad1/5$^+$, and p-Smad2$^+$ cell numbers were significantly lower in DMM/Cre mice than in DMM/GFP mice (Fig. 5*F-H, K, L*). Likewise, Trap staining showed a statistically significant decrease in Trap$^+$ cell numbers in DMM/Cre mice when compared with DMM/GFP mice (Fig. 5*I, K*).

Three-dimensional high-resolution μCT images of tibial subchondral bone medial compartment revealed that GFP-Cre-adenovirus instillation significantly restored DMM-induced Tb.Sp and DMM-negated SBP.Th, BV/TV, and Tb.N, when compared with GFP-adenovirus instillation (Fig. 5*J, M-O*). Thus, consistent with the *in vitro* roles of Cdc42 in TGF-β1-induced osteoblastogenesis, genetic disruption of *Cdc42* negated TGF-β1 signalling and subsequently attenuated subchondral bone remodelling in the experimental OA model.

Lentiviral Cdc42 knockdown attenuates articular cartilage degradation and subchondral bone deterioration in mice with experimental OA

We confirmed the roles of Cdc42 in articular cartilage degradation and subchondral bone deterioration in the experimental OA mouse model by intra-articular instillation of lentiviruses expressing GFP-scrambled-shRNA or GFP-Cdc42-shRNA into mice with sham or DMM operations. Lentiviral GFP was expressed in the same manner as adenoviral GFP in the knee joints of sham- and DMM-operated mice. Lentiviral Cdc42-shRNA had the same effects on articular cartilage degradation, IL-1β signalling, subchondral bone remodelling, and TGF-β1 signalling in DMM-operated

mice as observed in adenoviral GFP-Cre in DMM-operated *Cdc42*$^{flox/flox}$ mice (Supporting Fig. 4, 5). Thus, lentiviral knockdown of Cdc42 consistently attenuated articular cartilage degradation and subchondral bone deterioration in mice with experimental OA.

Inhibition of Cdc42 activity attenuates articular cartilage degradation in mice with experimental OA

We determined whether inhibition of Cdc42 activity was sufficient to attenuate articular cartilage degradation by intra-articular administration of ZCL278. Pilot studies using ZCL278 ranging from 2 to 16 μg per joint indicated that ZCL278 at 8 μg achieved a maximal protective effect against articular cartilage degradation in mice at 12 weeks post DMM operation (Supporting Fig. 6). We therefore used the ZCL278 at 8 μg per joint in the subsequent experiments. H&E and Safranin-O staining revealed severe structure loss in mice at 8 or 12 weeks post DMM operation, whereas ZCL278 administration attenuated this destruction to articular cartilage (Fig. 6*A-C*; Supporting Fig. 7*A-C*). Histomorphometric analyses further indicated that DMM surgery caused a robust decrease in the HC thickness but a marked increase in the CC thickness, whereas ZCL278 significantly restored these alterations in articular cartilage, as indicated by the reduced SS and MS of OA (Fig. 6*G, H*; Supporting Fig. 7*G, H*). Immunostaining and semi-quantification indicated that ZCL278 administration greatly diminished the expression of MMP13 and COLX in the articular and calcified cartilage (Fig.6*D, E, I*; Supporting Fig. 7*D, E, I*). Consistently, immunostaining and semi-quantification indicated that intra-articular administration of ZCL278 substantially diminished the numbers of p-Stat3^{+} cells in DMM-operated mice (Fig. 6*F, I*). Thus, intra-articular inhibition of Cdc42 activity potently attenuated articular cartilage degeneration in mice with experimental OA.

Inhibition of Cdc42 activity attenuates subchondral bone remodelling in mice with experimental OA

We determined whether inhibition of Cdc42 activity was sufficient to attenuate the subchondral bone remodelling in mice with experimental OA by μCT examination, immunostaining, and semi-quantification. Immunostaining revealed that ZCL278 treatment in DMM-operated mice significantly decreased the numbers of nestin$^+$, osterix$^+$, ALP$^+$, and VEGFR2$^+$ cells in subchondral bone marrow, when compared with a vehicle treatment (Fig. 7*A-D, J, K*). We also investigated the *in vivo* effects of ZCL278 on TGF-β1 signalling in subchondral bone areas. Immunostaining indicated that ZCL278 treatment of DMM-operated mice significantly decreased the numbers of p-Erk1/2$^+$, p-Smad1/5$^+$ and p-Smad2$^+$ cells when compared with a vehicle treatment (Fig. 7*E-G, J, K*). ZCL278 administration to DMM-operated mice also significantly decreased the numbers of Trap$^+$ cells when compared with vehicle administration (Fig. 7*H, J*). The μCT examination of the medial compartment of tibial subchondral bone also revealed that ZCL278 treatment significantly restored DMM-induced Tb.Sp and DMM-negated SBP.Th, BV/TV, and Tb.N, when compared with vehicle treatment (Fig. 7*I, L-N*; Supporting Fig. 7*F, J-L*). Thus, consistent with the *in vitro* results, inhibition of Cdc42 activity attenuated TGF-β1 signalling and subchondral bone remodelling in mice with experimental OA.

Discussion

The present study is the first to reveal critical roles for Cdc42 in both articular cartilage degeneration and subchondral bone deterioration in experimental OA. Specifically, both genetic disruption of *Cdc42* and inhibition of Cdc42 activity apparently attenuated the development of OA by reducing articular cartilage degeneration and subchondral bone sclerosis. The results also indicate that Cdc42 most likely lies upstream of Pak to induce IL-6 production and subsequently activates Jak/Stat3 in causing articular chondrocyte degradation during IL-1β signalling, whereas Cdc42 lies upstream of Erk to activate Smads in causing subchondral bone remodelling during TGF-β1 signalling (Fig. 8).

The DMM animal model provided extremely good reproducibility and a slower progression of OA disease, and closely resembled the more slowly-progressive human OA.[20] DMM mice with experimental OA showed high expression of Cdc42 in articular cartilage and subchondral bone. DNA arrays from human articular cartilage have identified cellular functions and biologic processes that are enriched in the superficial zone relative to the deep zone: most prominently, interferon, IL-4, Cdc42/Rac, and Jak/Stat signalling.[26] Our recent work and other previous studies have indicated that Cdc42 is critical for chondrocyte biological processes, including mesenchymal condensation, chondrogenesis, chondrocyte proliferation and apoptosis.[11-15] Genetic disruption of *Cdc42* or inhibition of Cdc42 activity also attenuated the articular chondrocytic hypertrophy observed in mice with experimental OA, in agreement with previous observations of reductions in COLX and MMP13 in non-resorbed hypertrophic cartilage in *Prx1Cre;Cdc42*$^{flox/flox}$ mice and inhibition of the terminal differentiation of chondrocytes by deletion of *Cdc42*.[12] The close association between Cdc42 activation and chondrocytic degradation is supported by

the observation that shear stress activates Cdc42 to induce MMP9 expression and IL-1β activates Rac1 to enhance the degradation in articular chondrocytes.[27, 28] However, in the work of Novakofski, it is demonstrated that IL-1α, IL-6 or IL-8 decreases GTP-Cdc42 and induces the degradation phenotypes in articular chondrocytes from pubescent horses.[18] The discrepancy between our and Novakofski's results is possibly due to the different sources of chondrocytes, stimulators, and culture conditions, and implies that the function and activity of Cdc42 are cell-context-dependent.

Activation of Cdc42 occurs at 30 min post IL-1β stimulation and IL-1β begins to induce Jak1/2 phosphorylation at 1 h post IL-1β treatment. Therefore, we infer that IL-1β directly activates Cdc42 that induces the production of IL-6 to activate Jak/Stat3. This notion is supported by our following findings: (1) IL-1β activates Cdc42 and induces IL-6 production, while inhibition of Cdc42 attenuates IL-1β-induced IL-6 production; (2) IL-6 is unable to activate Cdc42; (3) IL-6 neutralizing antibody is unable to block the IL-1β-induced Cdc42 activation but significantly diminishes IL-1β-induced Jak/Stat3 activation. Since Cdc42 is a critical regulator of the actin-mediated cytoskeleton formation and the actin cytoskeleton regulates chondrocyte differentiation,[29-32] a genetic disruption of *Cdc42* or inhibition of Cdc42 activity would suppress articular cartilage degradation, possibly through influences on the cytoskeleton. In addition, the TGF-β1-induced superficial zone protein (SZP) accumulation at the surface of articular cartilage depends on the cytoskeleton, whereas the small molecule Cdc42 inhibitor, ML141, inhibits SZP accumulation.[33] Therefore, Cdc42 is also likely to affect SZP synthesis and thereby induces articular degradation in OA.

Genetic disruption of *Cdc42* or inhibition of Cdc42 activity reduced the numbers of Trap$^+$ osteoclasts in mice with experimental OA, consistent with previous studies suggesting that Cdc42 regulates osteoclast formation and functions.[13,22] Abnormal angiogenesis in subchondral bone is one of the typical pathological features of OA. Elevated osteoclast activity induces the penetration of neovascular vessels from subchondral bone into the upper layer of the articular cartilage in OA, and nestin$^+$ MSCs are involved in this angiogenesis, as well as in osteoblast differentiation.[34-37] Our findings indicated that genetic disruption of *Cdc42* or inhibition of Cdc42 activity attenuates the formation of VEGFR2$^+$ and nestin$^+$ cells in subchondral bone, in agreement with previous studies demonstrating that Cdc42 participates in angiogenesis and is essential for neovascular formation in response to VEGF/VEGFR2 signalling that is critical for the development of OA.[38,39]

In response to an abnormal mechanical loading environment, subchondral bone undergoes modelling and remodelling, with aberrant activation of TGF-β signalling, resulting in bone resorption at the early stage of OA and excessive sclerotic bone formation (primarily due to nestin$^+$ MSC clusters) at the late stage of OA.[5,40] Consistent with the *in vitro* findings indicating that Cdc42 is critical for Smads activation and osteoblastogenesis in response to TGF-β1, genetic disruption of *Cdc42* or inhibition of Cdc42 activity attenuated the numbers of nestin$^+$ MSCs and effectively restored the recruitment of osterix$^+$ osteoprogenitors from the bone marrow to bone surface. We speculate that two mechanisms govern these effects: (1) decreased bone resorption due to Cdc42 inhibition possibly reduces the release of TGF-β1 and (2) inhibition of Cdc42/Erk-mediated smad2/3 and smad1/5 activation suppresses MSC condensation and osteoblast differentiation.

Cdc42 is essential for subchondral bone remodelling in mice with experimental OA, but our previous study indicates that Cdc42 is not involved in either bone formation in *collagen1α1Cre;Cdc42*$^{flox/flox}$ and *Prx1Cre;Cdc42*$^{flox/flox}$ mice or in osteoblastogenesis of cultured C3H10T1/2 cells.[11] This discrepancy supports a requirement for high activity of Cdc42 in subchondral bone areas of OA for bone remodelling in response to osteogenic stimulators, such as TGF-β1, whereas no similar requirement for basal levels of Cdc42 activity exists for bone formation.

Articular cartilage and subchondral bone act in concert as a functional unit in the joint, and biochemical and biomechanical crosstalk between them mediates the onset and development of OA.[1-3,37,38] Given that inhibition of Cdc42 completely attenuates articular cartilage degeneration and subchondral bone deterioration in OA, targeting Cdc42 appears to be a promising therapeutic approach for the OA treatment.

Disclosures

The authors declare that they have no conflict of interest.

Acknowledgments

We thank Dr. Yi Zheng (Department of Experimental Hematology and Cancer Biology, Cincinnati Children's Hospital Medical Center) for *Cdc42*$^{flox/flox}$ mice and Dr. Jianquan Chen (Orthopaedic Institute of Soochow University, China) for technical support. This work was supported by the National Natural Science Foundation of China (Nos. 31571493, 31271561, 31071292, 81171748, 81571928) and Department of Education of Zhejiang Province (Y201328229).

Authors' roles: XH, XJ, JW, and XW conceived and designed the experiments. XH, XJ, SF, JW, ML, WS, CX, and JD performed the experiments and analyzed the data. MY, LM, XF, and MH contributed the materials and reagents.

Supporting Information

Supporting Figures and Table can be found with this article online.

References

1. Kapoor M, Martel-Pelletier J, Lajeunesse D, et al. Role of proinflammatory cytokines in the pathophysiology of osteoarthritis. Nat Rev Rheumatol. 2011;7(1):33-42.
2. Moon P M, Beier F. Novel insights into osteoarthritis joint pathology from studies in mice. Curr Rheumatol Rep. 2015;17(8):50.
3. Lories RJ, Luyten FP. The bone-cartilage unit in osteoarthritis. Nat Rev Rheumatol 2011;7(1):43-9.
4. Pan J, Wang B, Li W, et al. Elevated cross-talk between subchondral bone and cartilage in osteoarthritic joints. Bone. 2012;51(2):212-7.
5. Zhen G, Wen C, Jia X, et al. Inhibition of TGF-[beta] signaling in mesenchymal stem cells of subchondral bone attenuates osteoarthritis. Nat Med. 2013;19(6):704-12.
6. Zhang L, Hu H, Tian F, et al. Enhancement of subchondral bone quality by alendronate administration for the reduction of cartilage degeneration in the early phase of experimental osteoarthritis. Clin Exp Med. 2011;11(4):235-43.
7. Wojdasiewicz P, Poniatowski ŁA, Szukiewicz D. The role of inflammatory and anti-inflammatory cytokines in the pathogenesis of osteoarthritis. Mediators inflamm. 2014;2014:561459.
8. Blasioli DJ, Kaplan DL. The roles of catabolic factors in the development of osteoarthritis. Tissue Eng Part B Rev. 2014;20(4):355-63.
9. Calich ALG, Domiciano DS, Fuller R. Osteoarthritis: can anti-cytokine therapy play a role in treatment? Clin Rheumatol. 2010;29(5):451-5.
10. Exton JH. Small GTPases minireview series. J Biol Chem. 1998;273(32):19923.
11. Wang JR, Wang CJ, Xu CY, et al. Signaling Cascades Governing Cdc42-Mediated Chondrogenic Differentiation and Mensenchymal Condensation. Genetics. 2016;202(3):1055-69.
12. Aizawa R, Yamada A, Suzuki D, et al. Cdc42 is required for chondrogenesis and interdigital programmed cell death during limb development. Mech Dev. 2012;129(1-4):38-50.
13. Suzuki W, Yamada A, Aizawa R, et al. Cdc42 is critical for cartilage development during endochondral ossification. Endocrinology. 2014;156(1):314-22.

14. Woods A, Wang G, Dupuis H, et al. Rac1 signaling stimulates N-cadherin expression, mesenchymal condensation, and chondrogenesis. J Biol Chem. 2007;282(32):23500-8.
15. Wang G, Beier F. Rac1/Cdc42 and RhoA GTPases antagonistically regulate chondrocyte proliferation, hypertrophy, and apoptosis. J Bone Miner Res. 2005;20(6):1022-31.
16. Ito Y, Teitelbaum SL, Zou W, et al. Cdc42 regulates bone modeling and remodeling in mice by modulating RANKL/M-CSF signaling and osteoclast polarization. J Clin Invest. 2010; 120(6):1981-93.
17. Abraham S, Scarcia M, Bagshaw RD, et al. A Rac/Cdc42 exchange factor complex promotes formation of lateral filopodia and blood vessel lumen morphogenesis. Nat Commun. 2015;6:7286.
18. Novakofski KD, Torre CJ, Fortier LA. Interleukin-1α, -6, and -8 decrease Cdc42 activity resulting in loss of articular chondrocyte phenotype. J Orthop Res. 2012;30(2):246-51.
19. Yang L, Wang L, Geiger H, et al. Rho GTPase Cdc42 coordinates hematopoietic stem cell quiescence and niche interaction in the bone marrow. Proc Natl Acad Sci 2007;104(12):5091-6.
20. Glasson SS, Blanchet TJ, Morris EA. The surgical destabilization of the medial meniscus (DMM) model of osteoarthritis in the 129/SvEv mouse. Osteoarthritis Cartilage 2007;15(9):1061-9.
21. Gosset M, Berenbaum F, Thirion S, et al. Primary culture and phenotyping of murine chondrocytes. Nat Protoc. 2008;3(8):1253-60.
22. Gong Y, Xu CY, Wang JR, et al. Inhibition of phosphodiesterase 5 reduces bone mass by suppression of canonical Wnt signaling. Cell Death Dis. 2014;5:e1544.
23. Yao H, Wei S, Wu J, et al. Endothelial Rac1 is essential for hematogenous metastasis to the lung. Oncotarget. 2015;6(19):17501-13.
24. Glasson SS, Chambers MG, Van Den Berg WB, et al. The OARSI histopathology initiative–recommendations for histological assessments of osteoarthritis in the mouse. Osteoarthritis Cartilage. 2010;18(Suppl 3): S17-23.
25. Bouxsein ML, Boyd SK, Christiansen BA, et al. Guidelines for assessment of bone microstructure in rodents using micro-computed tomography. J Bone Miner Res. 2010;25(7):1468-86.

26. Geng Y, Valbracht J, Lotz M. Selective activation of the mitogen-activated protein kinase subgroups c-Jun NH2 terminal kinase and p38 by IL-1 and TNF in human articular chondrocytes. J Clin Invest. 1996;98(10):2425-30.
27. Jin G, Sah RL, Li YS, et al. Biomechanical regulation of matrix metalloproteinase-9 in cultured chondrocytes. J Orthop Res. 2000;18(6):899-908.
28. Zhu S, Lu P, Liu H, et al. Inhibition of Rac1 activity by controlled release of NSC23766 from chitosan microspheres effectively ameliorates osteoarthritis development in vivo. Ann Rheum Dis. 2015;74(1):285-93.
29. Mori T, Miyamoto T, Yoshida H, et al. IL-1beta and TNFalpha-initiated IL-6-STAT3 pathway is critical in mediating inflammatory cytokines and RANKL expression in inflammatory arthritis. Int Immunol. 2011;23(11):701-12.
30. Legendre F, Dudhia J, Pujol JP, et al. JAK/STAT but not Erk1/Erk2 pathway mediates interleukin (IL)-6/soluble IL-6R down-regulation of Type II collagen, aggrecan core, and link protein transcription in articular chondrocytes. Association with a down-regulation of SOX9 expression. J Biol Chem. 2003;278(5):2903-12.
31. Kurgonaite K, Gandhi H, Kurth T, et al. Essential role of endocytosis for interleukin-4-receptor-mediated JAK/STAT signalling. J Cell Sci. 2015;128(20):3781-95.
32. Woods A, Wang G, Beier F. Regulation of chondrocyte differentiation by the actin cytoskeleton and adhesive interactions. J Cell Physiol. 2007;213(1):1-8.
33. Mcnary SM, Athanasiou KA, Reddi AH. Transforming growth factor β-induced superficial zone protein accumulation in the surface zone of articular cartilage is dependent on the cytoskeleton. Tissue Eng Part A. 2014;20(5-6):921-9.
34. Hayami T, Pickarski M, Wesolowski GA, et al. The role of subchondral bone remodeling in osteoarthritis: reduction of cartilage degeneration and prevention of osteophyte formation by alendronate in the rat anterior cruciate ligament transection model. Arthritis Rheum. 2004;50(4):1193-206.
35. Milgram JW. Morphologic alterations of the subchondrall bone in advanced degenerative arthritis. Clin Orthop Relat Res. 1983;173:293-312.
36. Ono N, Ono W, Mizoguchi T, et al. Vasculature-associated cells expressing nestin in developing bones encompass early cells in the osteoblast and endothelial lineage. Dev cell. 2014;29(3):330-9.

37. Zhou BO, Yue R, Murphy MM, et al. Leptin-receptor-expressing mesenchymal stromal cells represent the main source of bone formed by adult bone marrow. Cell stem cell. 2014;15(2):154-68.
38. Pfander D, Körtje D, Zimmermann R, et al. Vascular endothelial growth factor in articular cartilage of healthy and osteoarthritic human knee joints. Ann Rheum Dis. 2001;60(11):1070-3.
39. Enomoto H, Inoki I, Komiya K, et al. Vascular endothelial growth factor isoforms and their receptors are expressed in human osteoarthritic cartilage. Am J Path. 2003;162(1):171-81.
40. Cui Z, Crane J, Xie H, et al. Halofuginone attenuates osteoarthritis by inhibition of TGF-β activity and H-type vessel formation in subchondral bone. Ann Rheum Dis. 2015;75(9):1714-21.

Figure Legends

Fig. 1. Expression of Cdc42 in articular chondrocytes and subchondral bone and its involvements in IL-1β-induced inflammation. (*A*) Immunostaining for Cdc42 in knee joint sections of normal mice or mice at 8 weeks post sham or DMM operation. (*B*) Alizarin Red S staining and quantification in ATDC5 cells and PACs incubated with or without hypertrophic medium (HM) in the presence or absence of ZCL278 at 50 μM, for 21 and 14 days, respectively. (*C*) Pull-down assay for determination of GTP-Cdc42 levels in PACs treated with IL-1β at 10 ng/ml for 30 min. (*D, E*) Effect of ZCL278 and IPA-3 on activation of Jak1/2 and Stat3 by IL-1β. PACs were treated with IL-1β at 10 ng/ml for the indicated times or 1 h. (*F, G*) Effects of ZCL278 on *MMP13* and *COLX* mRNA levels in PACs. PACs were treated with IL-1β at 10 ng/ml for 24 h. (*H-J*) Synergistic effects of IPA-3 and ZCL278 on activation of Stat3 and mRNA expression of *MMP13* and *COLX*. PACs were treated with IL-1β at 10 ng/ml for 24 h. The indicated concentrations of ZCL278 or IPA-3 were incubated 2 h before and during IL-1β treatments. Immunoreactive bands from three independent experiments were quantified and the mean (n=3) intensity is presented under each band. Numerical data are presented as Means ± SEM (n=3); **p*<0.05, ***p*<0.01 versus vehicle treatment; $^{+}$ *p*<0.05, $^{++}$ *p*<0.01 versus HM or IL-1β treatment.

Fig. 2. Involvement of Cdc42 in IL-1β-induced IL-6 production and Jak/Stat3 activation. (*A, B*) Effects of ZCL278 on IL-1β-induced IL-6 mRNA expression. PACs were treated with IL-1β at 10 ng/ml for the indicated times or 1 h, ZCL278 at 20 (ZCL-20) or 50 (ZCL-50) μM were treated 2 h before and during IL-1β treatments. (*C, D*) Effects of ZCL278 and IPA-3 on IL-6 production in response to IL-1β stimulation. PACs were treated with IL-1β at 10 ng/ml for 1 h, and ZCL278 at 50 μM or IPA-3 at

20 μM was treated 2 h before or during IL-1β treatments, IL-6 levels in the culture media were determined by an ELISA kit and normalised to protein levels. (*E-G*) Effects of IL-6 and IL-6 neutralizing antibody (IL-6ab) on Cdc42 and Jak/Stat3 activation. PACs were treated with IL-6 at 10 ng/ml for the indicated times or treated with IL-1β at 10 ng/ml for 1h, IL-6ab at 5 ng/ml was incubated 2 h before and during IL-1β treatments. Cells were harvested for Cdc42 activation assays and western blotting, Immunoreactive bands from three independent experiments were quantified and the mean (n=3) intensity is presented under each band. Numerical data are presented as Means ± SEM (n=3); **p*<0.05, ***p*<0.01 versus vehicle treatment; $^{+}$ *p*<0.05, $^{++}$ *p*<0.01 versus IL-1β treatment.

Fig. 3. Effects of Cdc42 on TGF-β1-induced osteoblastogenesis. (*A*) Pull-down assay for GTP-Cdc42 levels after TGF-β1 treatment at 5 ng/ml for 30 min in C3H10T1/2 cells. (*B-E*) Effects of Cdc42 on TGF-β1 signalling. TGF-β1 treatments were performed at 5 ng/ml for the indicated times or 30 min, and inhibitors including ZCL278 or PD98059 were treated 2h before and during TGF-β1 treatments. (*F*) Activation of Erk and P38 at 48 h after transfection of myc-tagged Cdc42 or caCdc42. (*G*) Effects of PD98059 on Cdc42-induced activation of Smads. 48 h after transfection, cells were subjected to western blot assays, PD98059 were incubated right after transfection. (*H*) Co-immunoprecipitation of endogenous p-Erk in C3H10T1/2 cells overexpressing myc-tagged vector, Cdc42 or caCdc42. (*I*) Effects of ZCL278 on ALP and osterix mRNA levels in cells treated with TGF-β1 at 5 ng/ml for 24 h. (*J, K*) ALP staining and activity (numerical data) in C3H10T1/2 cells cultured in OBM/ZCL278 or transfected with caCdc42 for 7 days. (*L, M*) Effects of Cdc42 on the mRNA level of *Runx2* and *Col1a1* and mineralization in primary BMSCs. BMSCs

was incubated with TGF-β1 at 5 ng/ml for 24 h or OBM for 21 days in the presence or absence of ZCL278 at 50 μM. Immunoreactive bands from three independent experiments were quantified and the mean (n=3) intensity is presented under each band. Numerical data are presented as Means ± SEM (n=3); *p<0.05, **p<0.01 versus vehicle treatment or vector transfection; ^{+}p<0.05, ^{++}p<0.01 versus TGF-β1 or OBM treatment.

Fig. 4. Attenuation of articular cartilage degeneration by genetic disruption of *Cdc42* in *Cdc42*$^{flox/flox}$ mice. *Cdc42*$^{flox/flox}$ mice were intra-articularly injected with GFP- or GFP-Cre-expressing adenoviruses on day 10 post sham- or DMM-operation. The knee joints were harvested at 4, 8 and 12 weeks post-operation, followed by paraffin-embedded sectioning, histological examination, immunostaining and quantification. (*A-D, I, J*) Representative images for GFP, H&E, and Safranin-O fast green staining and the OARSI scoring in knee joints at 12 weeks post-DMM. (*E-H*, *K*) Immunostaining for Cdc42 (Cdc42^{+} cells/mm^{2}), MMP13 (MMP13^{+} cells%), COLX (COLX^{+} cells%) and p-Stat3 (p-Stat3^{+} cells/mm^{2}) and their quantification in sections of knee joints at 12 weeks post-DMM. Means ± SEM (n=5 for Sham/GFP group and n=9 for other groups); *p<0.05, **p<0.01 versus sham operation and GFP-adenovirus infection; ^{+}p<0.05, ^{++}p<0.01 versus DMM operation and GFP-adenovirus infection. Arrows denote the destruction and square frames define the magnified regions presented in (*D*).

Fig. 5. Disruption of subchondral bone microarchitecture by genetic disruption of *Cdc42* in *Cdc42*$^{flox/flox}$ mice. *Cdc42*$^{flox/flox}$ mice were intra-articularly injected with GFP- or GFP-Cre-expressing adenoviruses on day 10 post sham- or DMM-operation. The tibias were harvested at 4, 8 and 12 weeks post-operation, followed by μCT

examination, paraffin-embedded sectioning, immunostaining and quantification. (*A-E, K, L*) Immunostaining and quantification of Cdc42 ($Cdc42^+$ cells/mm^2), nestin ($Nest^+$ cells/mm^2), osterix (OSX^+ cells/mm^2), ALP (ALP^+ cells/mm^2), and VEGFR2 ($VEGFR2^+$ cells/mm^2) in subchondral bone at 8 weeks post-DMM. (*F-I, K, L*) Staining and quantification of p-Erk1/2 (p-Erk^+ cells/mm^2), p-Smad1/5 (p-$Smad1/5^+$ cells/mm^2), and p-Smad2 (p-$Smad2^+$ cells/mm^2) at 8 weeks post-DMM, and Trap (pink) of subchondral bone at 4 weeks post-DMM. (*J, M-O*) μCT images and quantifications of the tibial subchondral bone medial compartment of mice at 12 weeks post-operation. Means ± SEM (n=5 for Sham/GFP group and n=9 for other groups); **p*<0.05, ***p*<0.01 versus sham operation and GFP-adenovirus infection; ^{+}p<0.05, ^{++}p<0.01 versus DMM operation and GFP-adenovirus infection.

Fig. 6. Attenuation of articular cartilage degeneration by ZCL278 in DMM-operated mice. Mice were intra-articularly injected with vehicle or ZCL278 on day 10 post sham or DMM operation. The knee joints were harvested at 4, 8 and 12 weeks post-operation, followed by paraffin-embedded sectioning, histological examination, immunostaining and quantification. (*A-C, G, H*) H&E and Safranin-O fast green staining for OARSI scoring in knee joints at 12 weeks post-DMM. (*D-F, I*) Immunostaining and quantification for MMP13, COLX and p-Stat3 in sections of knee joints at 12 weeks post-DMM. Means ± SEM (n=5 for Sham/vehicle group and n=9 for other groups); **p*<0.05, ***p*<0.01 versus sham operation and vehicle treatment; ^{+}p<0.05, ^{++}p<0.01 versus DMM operation and vehicle treatment. Arrows denote areas of destruction and square frames define the magnified regions presented in (*C*).

Fig. 7. Attenuation of subchondral bone deterioration by ZCL278 in DMM-operated mice. Mice were intra-articularly injected with vehicle or ZCL278 on day 10 post sham or DMM operation. Tibias were paraffin-embedded, sectioned and stained and also subjected to μCT. (*A-E, J, K*) Immunostaining and quantification for nestin, osterix, VEGFR2, ALP, and p-Erk1/2 in tibial subchondral bone at 8 weeks post-operation. (*F, G, K*) Immunostaining and quantification for p-Smad1/5 and p-Smad2. (*H, J*) Trap staining and quantification in tibial subchondral bone at 4 weeks post-operation. (*I, L-N*) μCT image and quantification of the tibial subchondral bone medial compartment of mice at 12 weeks post-operation. Means ± SEM (n=5 for Sham/vehicle group and n=9 for other groups); *p<0.05, **p<0.01 versus sham operation and vehicle treatment; ^{+}p<0.05, ^{++}p<0.01 versus DMM operation and vehicle treatment.

Fig. 8. A working model for the roles of Cdc42 in osteoarthritis. In articular cartilage degradation, Cdc42 lies on the upstream of Pak to induce the IL-6 production and subsequent Jak/Stat3 activation in response to IL-1β stimulation. In subchondral bone deterioration, Cdc42 lies on the upstream of Erk1/2 to activate Smads in response to TGF-β1 stimulation.

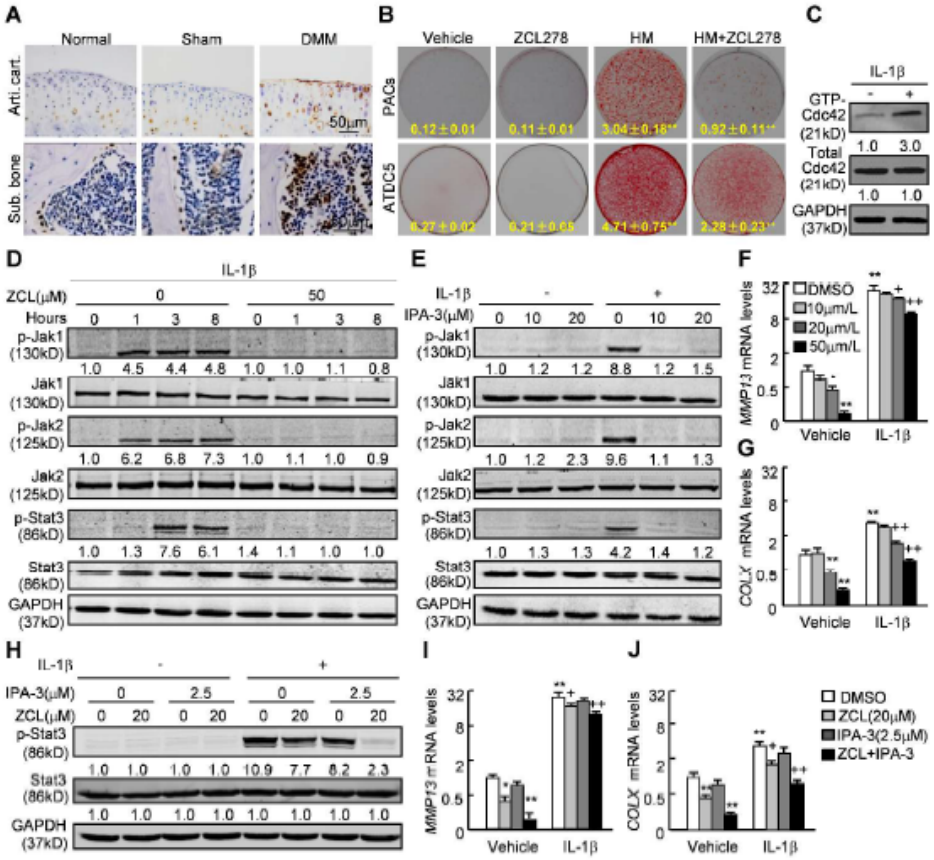

Fig. 1. Expression of Cdc42 in articular chondrocytes and subchondral bone and its involvements in IL-1β-induced inflammation. (A) Immunostaining for Cdc42 in knee joint sections of normal mice or mice at 8 weeks post sham or DMM operation. (B) Alizarin Red S staining and quantification in ATDC5 cells and PACs incubated with or without hypertrophic medium (HM) in the presence or absence of ZCL278 at 50 μM, for 21 and 14 days, respectively. (C) Pull-down assay for determination of GTP-Cdc42 levels in PACs treated with IL-1β at 10 ng/ml for 30 min. (D, E) Effect of ZCL278 and IPA-3 on activation of Jak1/2 and Stat3 by IL-1β. PACs were treated with IL-1β at 10 ng/ml for the indicated times or 1 h. (F, G) Effects of ZCL278 on MMP13 and COLX mRNA levels in PACs. PACs were treated with IL-1β at 10 ng/ml for 24 h. (H-J) Synergistic effects of IPA-3 and ZCL278 on activation of Stat3 and mRNA expression of MMP13 and COLX. PACs were treated with IL-1β at 10 ng/ml for 24 h. The indicated concentrations of ZCL278 or IPA-3 were incubated 2 h before and during IL-1β treatments. Immunoreactive bands from three independent experiments were quantified and the mean (n=3) intensity is presented under each band. Numerical data are presented as Means ± SEM (n=3); *p<0.05, **p<0.01 versus vehicle treatment; + p<0.05, ++ p<0.01 versus HM or IL-1β treatment.

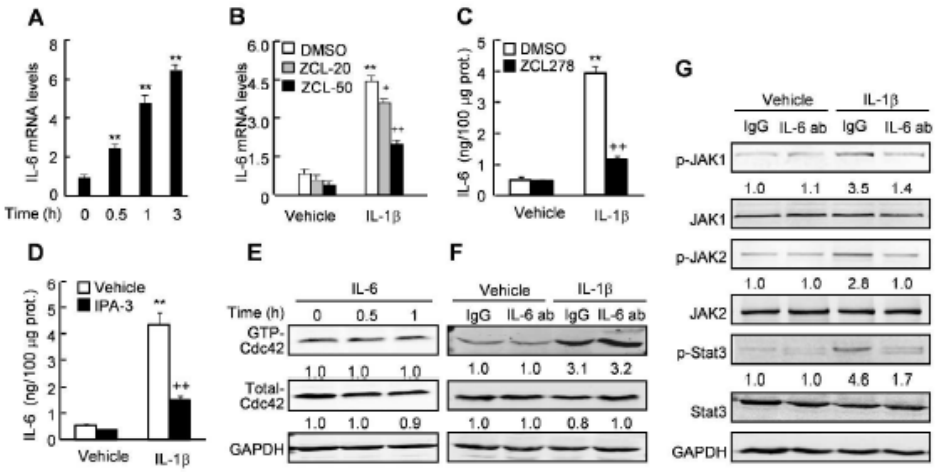

Fig. 2. Involvement of Cdc42 in IL-1β-induced IL-6 production and Jak/Stat3 activation. (A, B) Effects of ZCL278 on IL-1β-induced IL-6 mRNA expression. PACs were treated with IL-1β at 10 ng/ml for the indicated times or 1 h, ZCL278 at 20 (ZCL-20) or 50 (ZCL-50) μM were treated 2 h before and during IL-1β treatments. (C, D) Effects of ZCL278 and IPA-3 on IL-6 production in response to IL-1β stimulation. PACs were treated with IL-1β at 10 ng/ml for 1 h, and ZCL278 at 50 μM or IPA-3 at 20 μM was treated 2 h before or during IL-1β treatments, IL-6 levels in the culture media were determined by an ELISA kit and normalised to protein levels. (E-G) Effects of IL-6 and IL-6 neutralizing antibody (IL-6ab) on Cdc42 and Jak/Stat3 activation. PACs were treated with IL-6 at 10 ng/ml for the indicated times or treated with IL-1β at 10 ng/ml for 1h, IL-6ab at 5 ng/ml was incubated 2 h before and during IL-1β treatments. Cells were harvested for Cdc42 activation assays and western blotting. Immunoreactive bands from three independent experiments were quantified and the mean (n=3) intensity is presented under each band. Numerical data are presented as Means ± SEM (n=3); *p<0.05, **p<0.01 versus vehicle treatment; + p<0.05, ++ p<0.01 versus IL-1β treatment.

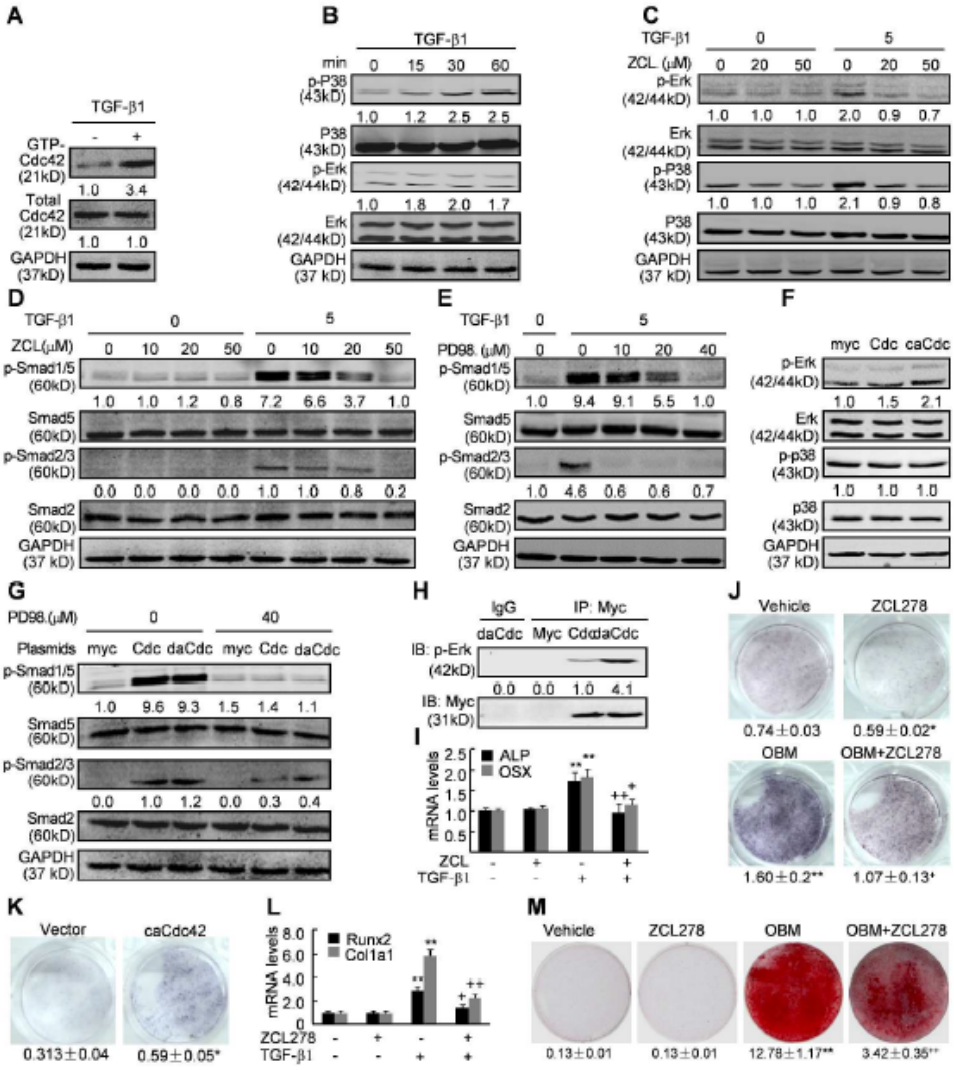

Fig. 3. Effects of Cdc42 on TGF-β1-induced osteoblastogenesis. (A) Pull-down assay for GTP-Cdc42 levels after TGF-β1 treatment at 5 ng/ml for 30 min in C3H10T1/2 cells. (B-E) Effects of Cdc42 on TGF-β1 signalling. TGF-β1 treatments were performed at 5 ng/ml for the indicated times or 30 min, and inhibitors including ZCL278 or PD98059 were treated 2h before and during TGF-β1 treatments. (F) Activation of Erk and P38 at 48 h after transfection of myc-tagged Cdc42 or caCdc42. (G) Effects of PD98059 on Cdc42-induced activation of Smads. 48 h after transfection, cells were subjected to western blot assays, PD98059 were incubated right after transfection. (H) Co-immunoprecipitation of endogenous p-Erk in C3H10T1/2 cells overexpressing myc-tagged vector, Cdc42 or caCdc42. (I) Effects of ZCL278 on ALP and osterix mRNA levels in cells treated with TGF-β1 at 5 ng/ml for 24 h. (J, K) ALP staining and activity (numerical data) in C3H10T1/2 cells cultured in OBM/ZCL278 or transfected with caCdc42 for 7 days. (L, M) Effects of Cdc42 on the mRNA level of Runx2 and Col1a1 and mineralization in primary BMSCs. BMSCs was incubated with TGF-β1 at 5 ng/ml for 24 h or OBM for 21 days in the presence or absence of ZCL278 at 50 μM. Immunoreactive bands from three independent experiments were quantified and the mean (n=3) intensity is presented under each band. Numerical data are presented as Means ± SEM (n=3); *p<0.05, **p<0.01 versus vehicle treatment or vector transfection; + p<0.05, ++ p<0.01 versus TGF-β1 or OBM treatment.

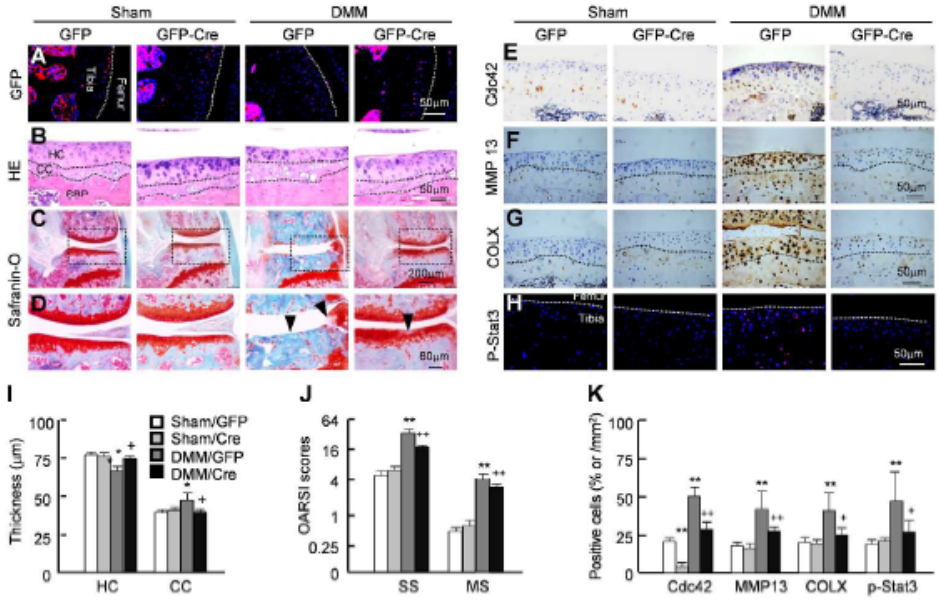

Fig. 4. Attenuation of articular cartilage degeneration by genetic disruption of Cdc42 in Cdc42flox/flox mice. Cdc42flox/flox mice were intra-articularly injected with GFP- or GFP-Cre-expressing adenoviruses on day 10 post sham- or DMM-operation. The knee joints were harvested at 4, 8 and 12 weeks post-operation, followed by paraffin-embedded sectioning, histological examination, immunostaining and quantification. (A-D, I, J) Representative images for GFP, H&E, and Safranin-O fast green staining and the OARSI scoring in knee joints at 12 weeks post-DMM. (E-H, K) Immunostaining for Cdc42 (Cdc42+ cells/mm2), MMP13 (MMP13+ cells%), COLX (COLX+ cells%) and p-Stat3 (p-Stat3+ cells/mm2) and their quantification in sections of knee joints at 12 weeks post-DMM. Means ± SEM (n=5 for Sham/GFP group and n=9 for other groups); *p<0.05, **p<0.01 versus sham operation and GFP-adenovirus infection; +p<0.05, ++p<0.01 versus DMM operation and GFP-adenovirus infection. Arrows denote the destruction and square frames define the magnified regions presented in (D).

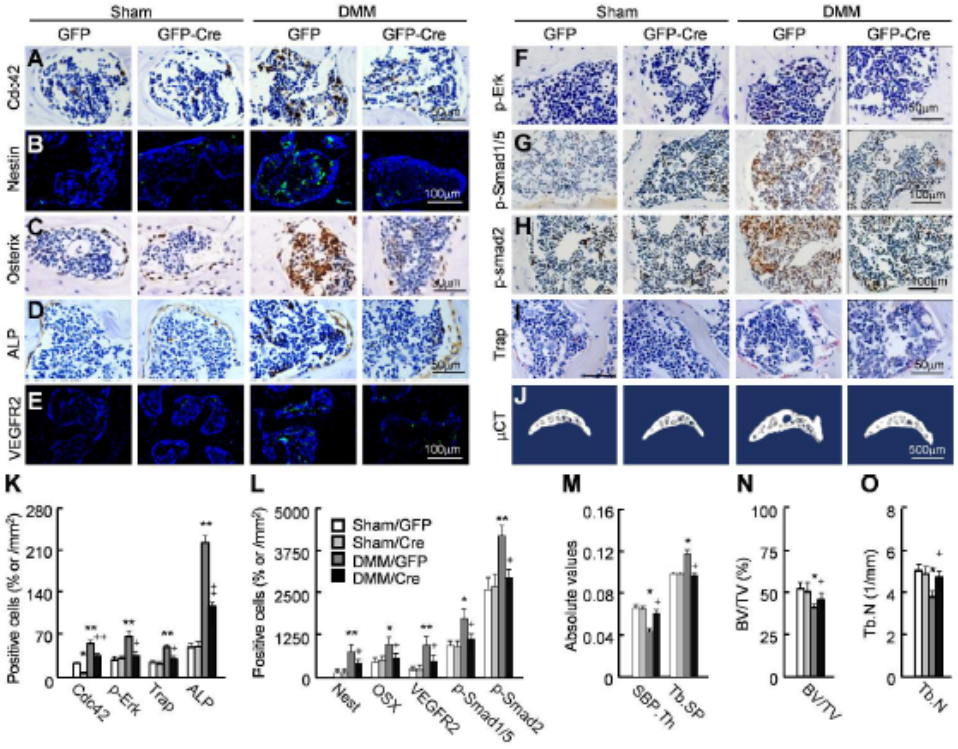

Fig. 5. Disruption of subchondral bone microarchitecture by genetic disruption of Cdc42 in Cdc42flox/flox mice. Cdc42flox/flox mice were intra-articularly injected with GFP- or GFP-Cre-expressing adenoviruses on day 10 post sham- or DMM-operation. The tibias were harvested at 4, 8 and 12 weeks post-operation, followed by μCT examination, paraffin-embedded sectioning, immunostaining and quantification. (A-E, K, L) Immunostaining and quantification of Cdc42 (Cdc42+ cells/mm2), nestin (Nest+ cells/mm2), osterix (OSX+ cells/mm2), ALP (ALP+ cells/mm2), and VEGFR2 (VEGFR2+ cells/mm2) in subchondral bone at 8 weeks post-DMM. (F-I, K, L) Staining and quantification of p-Erk1/2 (p-Erk+ cells/mm2), p-Smad1/5 (p-Smad1/5+ cells/mm2), and p-Smad2 (p-Smad2+ cells/mm2) at 8 weeks post-DMM, and Trap (pink) of subchondral bone at 4 weeks post-DMM. (J, M-O) μCT images and quantifications of the tibial subchondral bone medial compartment of mice at 12 weeks post-operation. Means ± SEM (n=5 for Sham/GFP group and n=9 for other groups); *p<0.05, **p<0.01 versus sham operation and GFP-adenovirus infection; +p<0.05, ++p<0.01 versus DMM operation and GFP-adenovirus infection.

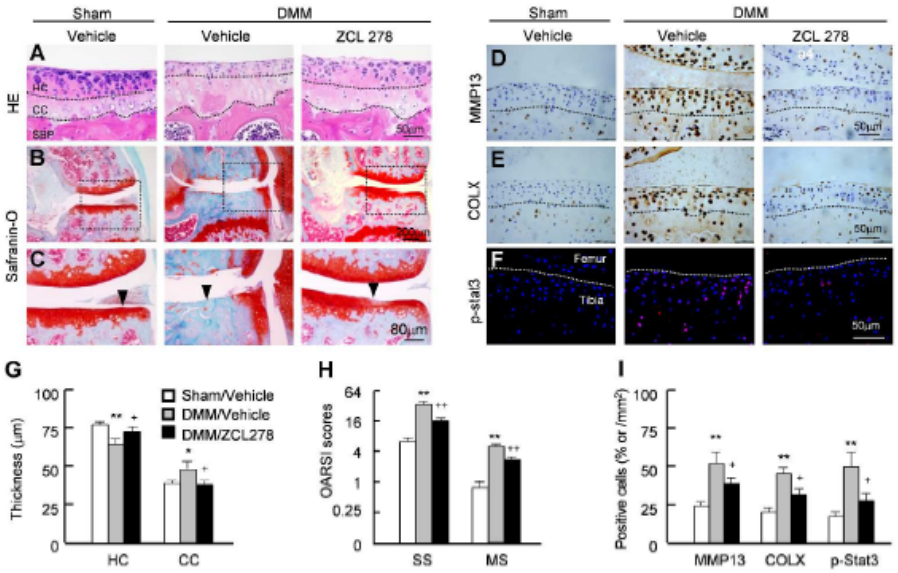

Fig. 6. Attenuation of articular cartilage degeneration by ZCL278 in DMM-operated mice. Mice were intra-articularly injected with vehicle or ZCL278 on day 10 post sham or DMM operation. The knee joints were harvested at 4, 8 and 12 weeks post-operation, followed by paraffin-embedded sectioning, histological examination, immunostaining and quantification. (A-C, G, H) H&E and Safranin-O fast green staining for OARSI scoring in knee joints at 12 weeks post-DMM. (D-F, I) Immunostaining and quantification for MMP13, COLX and p-Stat3 in sections of knee joints at 12 weeks post-DMM. Means ± SEM (n=5 for Sham/vehicle group and n=9 for other groups); *p<0.05, **p<0.01 versus sham operation and vehicle treatment; +p<0.05, ++p<0.01 versus DMM operation and vehicle treatment. Arrows denote areas of destruction and square frames define the magnified regions presented in (C).

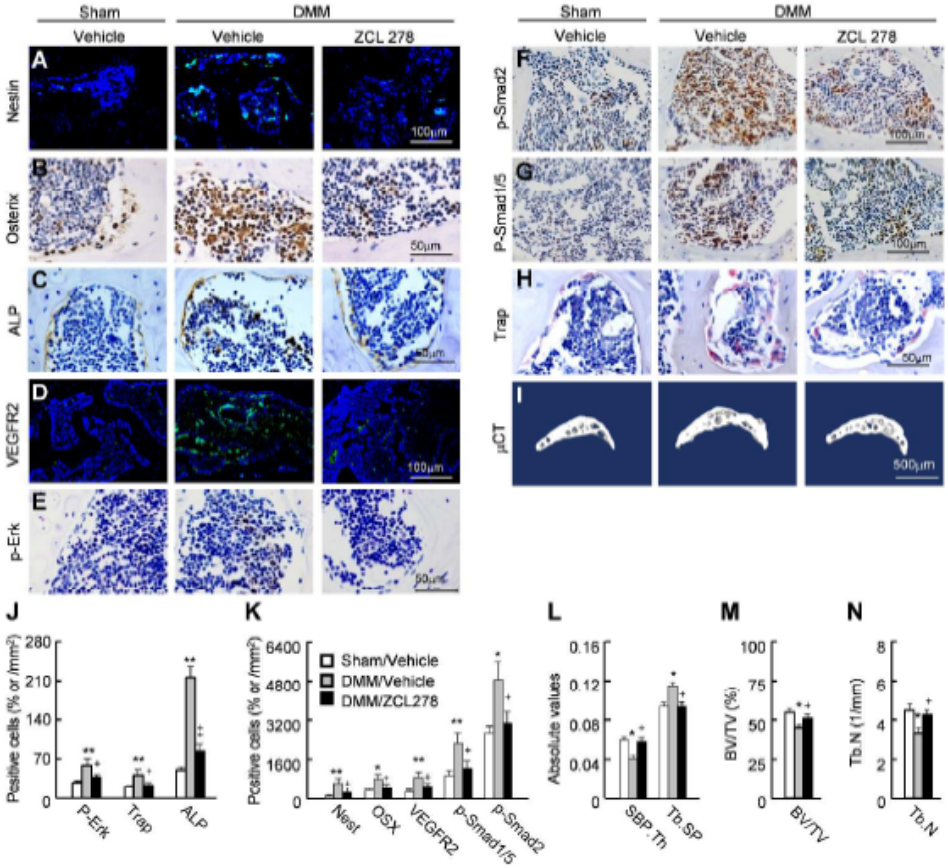

Fig. 7. Attenuation of subchondral bone deterioration by ZCL278 in DMM-operated mice. Mice were intra-articularly injected with vehicle or ZCL278 on day 10 post sham or DMM operation. Tibias were paraffin-embedded, sectioned and stained and also subjected to μCT. (A-E, J, K) Immunostaining and quantification for nestin, osterix, VEGFR2, ALP, and p-Erk1/2 in tibial subchondral bone at 8 weeks post-operation. (F, G, K) Immunostaining and quantification for p-Smad1/5 and p-Smad2. (H, J) Trap staining and quantification in tibial subchondral bone at 4 weeks post-operation. (I, L-N) μCT image and quantification of the tibial subchondral bone medial compartment of mice at 12 weeks post-operation. Means ± SEM (n=5 for Sham/vehicle group and n=9 for other groups); *p<0.05, **p<0.01 versus sham operation and vehicle treatment; +p<0.05, ++p<0.01 versus DMM operation and vehicle treatment.

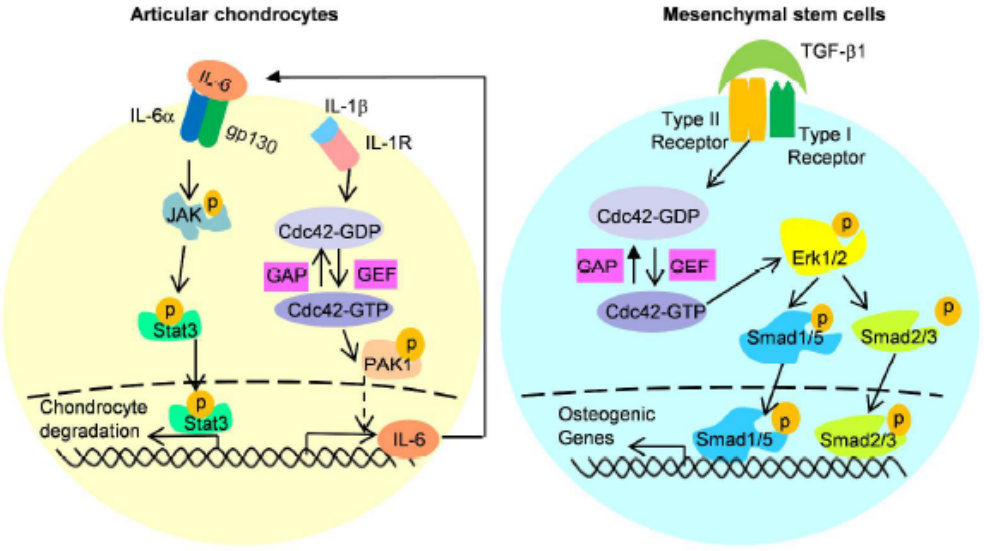

Fig. 8. A working model for the roles of Cdc42 in osteoarthritis. In articular cartilage degradation, Cdc42 lies on the upstream of Pak to induce the IL-6 production and subsequent Jak/Stat3 activation in response to IL-1β stimulation. In subchondral bone deterioration, Cdc42 lies on the upstream of Erk1/2 to activate Smads in response to TGF-β1 stimulation.